Influence of Arch Support Heights on the Internal Foot Mechanics of Flatfoot during Walking: A Muscle-Driven Finite Element Analysis

Yinghu Peng [a], Duo Wai-Chi Wong [a,b], Tony Lin-Wei Chen [a], Yan Wang [a,b], Guoxin Zhang [a], Fei Yan [a], Ming Zhang [a,b*]

[a] Department of Biomedical Engineering, Faculty of Engineering, The Hong Kong Polytechnic University, Hong Kong, China

[b] The Hong Kong Polytechnic University Shenzhen Research Institute, Shenzhen, China

*Corresponding author: Prof. Ming Zhang

Department of Biomedical Engineering, Faculty of Engineering,

The Hong Kong Polytechnic University,

Hung Hom, KLN,

Hong Kong, China

Email: ming.zhang@polyu.edu.hk

Abstract

Background

Different arch support heights of the customized foot orthosis could produce different effects on the internal biomechanics of the foot. However, quantitative evidence is scarce. Therefore, we aimed to investigate and quantify the influence of arch support heights on the internal foot biomechanics during walking stance.

Methods

We reconstructed a foot finite element model from a volunteer with flexible flatfoot. The model enabled a three-dimensional representation of the plantar fascia and its interactions with surrounding osteotendinous structures. The volunteer walked in foot orthosis with different arch heights (low, neutral, and high). Muscle forces during gaits were calculated by a multibody model and used to drive a foot finite element model. The foot contact pressures and plantar fascia strains in different regions were compared among the insole conditions at the first and second vertical ground reaction force (VGRF) peak and VGRF valley instants.

Results

The results indicated that peak foot pressures decreased in balanced standing and second VGRF as the arch support height increased. However, peak midfoot pressures increased during all simulated instants. Meanwhile, high arch support decreased the plantar fascia loading by 5% to 15.4 % in proximal regions but increased in the middle and distal regions.

Conclusion

Although arch support could generally decrease the plantar foot pressure and plantar fascia loading, the excessive arch height may induce high midfoot pressure and loadings at the central portion of the plantar fascia. The consideration of fascia-soft tissue interaction in modeling could improve the prediction of plantar fascia strains towards design optimization for orthoses.

1. Introduction

Adult-acquired flatfoot (AAF) is a common foot pathology defined by loss of the medial longitudinal arch during static and dynamic conditions with symptomatic progressive foot deformity [1]. The prevalence of AAF ranges from 19% to 27% [2, 3] and could reach 37% in patients with comorbidities [4]. The insufficiency of the foot arch in AFF affects the shock absorption capability and foot posture during weight-bearing, thereby contributing to lower limb dysfunction and low-quality life [1]. Clinical studies have shown that flatfoot is associated with other lower limb problems, including ankle pain and plantar fasciitis [5]. Efficient and timely treatments could slow down the progression of the deformity and improve the life quality. Foot orthoses are frequently prescribed to provide stability and pain relief by adjusting foot posture and lower limb alignment for early stage AFF [6].

Both custom-made and prefabricated insoles have been used to modify the foot posture and relieve pain in individuals with flexible flatfoot [7, 8]. Customized insoles are more effective than prefabricated insoles and offer better comfort for flatfoot patients [9, 10]. Additionally, customized insoles can relieve foot pain and improve the function of runners with running-related overuse injuries, such as plantar fasciitis [11]. However, the customized-insole design largely depends on the experience of the orthotist, which is subjective and qualitative [10]. Although studies have investigated the effects of foot orthosis design on flatfoot kinematics and kinetics, quantitative estimates of internal foot mechanics under various orthosis designs remain scarce [8, 12, 13]. Therefore, it is necessary to investigate the effects of different orthotic design

features, such as arch support, on plantar fascia loading.

Some studies have used cadaver experiments and in-vivo measurement methods to investigate internal foot biomechanics [14, 15]; however, it is challenging to systematically evaluate the ankle-foot complex load distribution, such as the distribution of plantar fascia strain. The finite element (FE) approach is among the most common computational approaches used to investigate comprehensive internal foot biomechanical responses to various loading conditions [16]. The FE model was adopted to investigate the effects of orthotic insoles on foot plantar pressure [17-20]. Simultaneously, studies were conducted to reduce plantar fascia stress and peak plantar pressure by redesigning the insole [17, 20]. The influence of arch support height on the plantar fascia stress was also investigated [21]. However, the plantar fascia has been conventionally simplified as truss elements [17, 22, 23], which cannot sufficiently demonstrate the distribution of fascia stress and strain. Although some studies reconstructed detailed three-dimensional (3D) plantar fascia [24, 25], the interaction between bulk soft tissue and plantar fascia was ignored, which might underestimate the plantar fascia loading [26]. A foot FE model with both fascia-bone and fascia-bulk soft tissue interactions could more reliably predict internal foot mechanics and provide evidence-based information to optimize insoles and improve functional outcomes.

To investigate the dynamic effects of insoles during walking, dynamic boundary conditions, including the muscle force and ground reaction force, were necessary for the foot FE model. However, measuring the in-vivo foot muscle force is challenging. Most studies have used muscle force derived from literature data [20] or simplified

loading conditions, such as static loading [17, 22, 23] in the foot-orthosis FE model. The combined musculoskeletal and FE model of the same participant could provide subject-specific boundary conditions for the foot-ankle complex model, thus improving the accuracy of predictions [25, 27]. The effects of arch support height on the internal foot dynamics in patients with flatfoot could be evaluated using the muscle-driven foot-orthosis FE model.

Therefore, this study aimed to investigate the effects of different arch support heights on the internal foot mechanics of flatfoot during walking based on a muscle-driven flatfoot FE model. We reconstructed a flatfoot FE model with 3D plantar fascia geometry using magnetic resonance imaging (MRI). Gait data were used as inputs for the musculoskeletal multibody model to calculate foot muscle forces. The calculated foot muscle forces and measured ground reaction forces were used to drive the flatfoot FE model. The calculated plantar fascia loading and foot contact pressure could help improve the insole design, particularly in patients with symptomatic flatfoot.

2. Methods

2.1 Participant information

A young male adult (age: 27 years, height: 175 cm, weight: 64 kg) with flexible flatfoot was recruited for this study. The participant had no neuromuscular disease or biomechanical abnormalities other than the flatfoot. In this study, the navicular drop test [28] and footprint index [29] were used to classify the foot type. Flatfoot is characterized by a high navicular drop (>10 mm) and footprint index (>0.26) [28, 29]. The participant's right foot was recognized as flatfoot with an arch index of 0.30 and a

navicular drop of 12 mm. Experimental data, including marker trajectories, ground reaction forces, foot pressure data, and MRI of the right foot, were collected.

2.2 Equipment and procedure

A 3D foot surface scanner (UPOD-HDS; ScanPod3D, Wuhan, China) was used to facilitate the insole design. A surface scan of the right foot was performed under minimal weight-bearing condition. For the minimal weight scan, the participant sat on a chair, and his shank was perpendicular to the surface of the scanner. In clinical practice, most orthotic insoles are produced based on minimal weight conditions. The overall thickness of the insole was 7 mm. As the participant's arch height was approximately 38 mm under the minimal weight-bearing condition, the initial total arch height was set at 45 mm. We conducted a sensitivity test on the arch support heights with reference to the initial arch height, including 42 mm for a low arch (LA), 45mm for a neutral arch (NA), and 48 mm for a high arch (HA). The scanned foot surface was further processed in Rapidform XOR2 (3D Systems Korea Inc., Seoul Korea) and output as a solid geometry. The insole profile was constructed using computer-aided design software (SolidWorks, Dassault Systèmes, Tennessee) based on the foot shape, as shown in Fig. 1(B). An orthotist and a therapist guided all these settings. As shown in Fig. 1(D), the insoles were fabricated using thermoplastic polyurethane (IROPRINT™ F80213, Huntsman, Belgium) through the fused deposition modeling (FDM) technology (Ultimaker S5, Utrecht, Netherlands). The 3D printing configuration included a nozzle temperature of 230 °C, printing speed of 50 mm/min, layer thickness of 0.2 mm, nozzle diameter of 0.4 mm, and filling rate of 30%. The

experimental effective elastic modulus and Poisson's ratio of the insoles were obtained using the Instron Machine (AG-IS, SHMADZU, Japan). The test was performed based on the compression testing standard ASTM D695 with a compressive speed of 1 mm/min and sampling frequency of 50 Hz. Five cylinder samples with a diameter of 12.7 mm and height of 25.4 mm were tested, and the average value was calculated. A pair of customized shoes (Dr Kong, HK, China) with holes was manufactured for the experiment (Fig. 1(C)).

Gait analysis was conducted in a laboratory with an eight-camera Vicon system (Vicon, Oxford Metrics Ltd., Oxford, England) and four force plates (OR6, AMTI, Watertown, United States). The equipment was used to capture marker trajectories and ground reaction forces. Marker trajectories and force plate data were collected synchronously at sampling frequencies of 100 Hz and 1000 Hz, respectively. Reflective markers were placed on the lower limb according to protocol [13]. Before the experiment, the participant had sufficient time to familiarize with the laboratory environment. Foot orthoses with three arch heights were randomly tested with rest intervals of 5 min. A static trial and five successful walking trials were conducted for each insole condition. The trials were considered successful when the footsteps were consistent, and foot was placed entirely within the force plates. Kinesiological electromyography (Delsys Inc., Boston, MA) was used to measure surface electromyography (EMG) signals, including the gastrocnemius medialis (GM), gastrocnemius lateralis (GL), tibialis anterior (TA), soleus (SL), and peroneus longus (PL). The foot pressure measurement system F-scan (Tekscan Inc., Boston, USA) was

used to obtain the in-shoe plantar pressure (Fig. 1(A)). During gait analysis, the foot

pressures under both static and dynamic conditions were collected. The experimental

setup is shown in Fig. 1.

2.3 Musculoskeletal multibody model

The collected gait data, including marker trajectories and force plate data, were

used to drive the musculoskeletal multibody model. A generic lower limb

musculoskeletal multibody model in the software (Anybody Technology, Aalborg,

Denmark, version 6.0.5) was used to calculate the lower limb's kinetics and kinematics

during walking [30]. The generic lower limb model was built based on the

anthropometric database of the Twente Lower Extremity Model, including a spherical

hip joint, hinged patellofemoral, tibiofemoral, ankle, and subtalar joints, and

approximately 160 muscle units [31]. The general lower limb model was scaled to

obtain the participant's model using the static trial. Inverse kinematic and inverse

dynamics analyses were then performed on the musculoskeletal multibody model using

the marker trajectories and force plate data as inputs. The joint contact forces and

muscle forces were estimated using muscle recruitment criteria [13].

2.4 Finite element model

2.4.1 Geometry acquisition and model construction

Right-foot MRI was performed with a 3.0-T MR scanner at an interval of 1 mm

and a pixel size resolution of 0.625 mm (Seimens, Erlangen, Germany). A custom

ankle-foot orthosis was used during the MRI scan to fix the ankle joint in a neutral,

unloaded position. The geometries of the foot-ankle complex, including the

encapsulated bulk tissue and twenty bone geometries, were reconstructed using medical image processing software (Mimics 10.1, Materialize Inc., Belgium). The bulk soft tissue was encapsulated by a 2-mm membrane, which defined the skin layer. We modeled 110 trusses to represent the ligamentous structure connected to the bones, whereas the plantar fascia was modeled as a 3D solid. The bulk soft tissue was obtained by subtracting the geometry of the plantar fascia. The plantar fascia was tied to the calcaneal tuberosity, proximal phalanx, and the inner surface of bulk soft tissues. Moreover, foot muscles were modeled as connectors to facilitate the application of muscle force. The tibialis anterior, tibialis posterior, peroneus brevis, peroneus longus, Achilles tendon (gastrocnemius and soleus), flexor hallucis longus, and flexor digitorum longus were considered in this model. They were reconstructed based on the MRI scans and confirmed by an orthopedic surgeon.

The interaction between the interior surface of the encapsulated soft tissue and bone was defined using a "tied" operation. A similar operation was performed to connect the 3D plantar fascia to the relevant insertion points, including the calcaneal tubercle and proximal phalanges. Additionally, the surface of the plantar fascia was tied to the surrounding encapsulated soft tissue. For the contact between components, a nonlinear contact stiffness without friction was used to represent the function of the cartilage (bone-bone contact) [32]. Fig. 2 shows the detailed foot FE configurations.

The mesh creation process was performed in Abaqus 6.14 (Simulia, Dassault Systèmes, France). Hexahedral elements were assigned to the ground plate in this study. Linear tetrahedral elements (C3D4) were used to mesh the bones, encapsulated bulk

tissue, insole, shoe, and plantar fascia. Three-node triangular membrane elements (M3D3) and two-node linear three-dimensional elements (T3D2) were assigned to the skin and linear ligaments, respectively. All foot-ankle complex material properties were assigned according to the literature [33-39]. The properties of the materials used in this study are listed in Table 1.

The overall element size was 3 mm for the bone structures, insole, shoe and plantar fascia and 5 mm for the encapsulated foot soft tissue and ground plate. The elements were refined locally to accommodate small part geometries, contact regions, and abrupt geometrical changes. The mesh convergence test was conducted under balancing standing conditions with a reduction in element size of 10%. The deviations of the peak foot pressure in the three insoles were 2.4% - 4.7%. The mesh size in the current simulation was acceptable as the deviations were smaller than 5% [40].

2.4.2 Boundary and loading conditions

The internal foot biomechanics were investigated at three gait instants during walking: the first peak vertical ground reaction force (VGRF), VGRF valley, and second peak VGRF (Fig. 3). The proximal cross-sectional surfaces of the tibia and fibula were fixed at all degrees of freedom. Additionally, a rigid plate was tied to the ground plate to better control the motion of the ground plate. The 3D ground reaction forces were applied beneath the rigid plate. The relative orientation between ground and foot was assigned based on the gait analysis data at the three gait instants. The calculated foot muscle forces, including the tibialis anterior, tibialis posterior, peroneus brevis, peroneus longus, Achilles tendon (gastrocnemius and soleus), flexor hallucis

longus, and flexor digitorum longus, were applied to the FE model through the defined muscle connectors. More information about the boundary conditions has been added in the Supplementary File 1. Fig. 4 illustrates further details of the muscle-driven FE model.

2.4.3 Model output and analysis

The simulations were performed with Abaqus 6.14 (Dassault Systèmes, Vélizy-Villacoublay, France) using the standard static solver. A parametric study was carried out at the three different arch support heights during walking. The walking speeds for LA, NA, and HA conditions were 1.39 m/s, 1.44 m/s, and 1.42 m/s, respectively. The foot contact pressures at the three gait instants, including the first peak VGRF, VGRF valley, and second peak VGRF, were obtained. The entire foot was divided into three parts: the hindfoot, midfoot, and forefoot area. The principal tensile strain of the 3D plantar fascia was also reported. Several main ligaments, including the calcaneocuboid, calcaneocuboid, deltoid, long plantar, cuboideonavicular, short plantar, and talonavicular ligaments, were significant in maintaining the foot posture. Therefore, the maximum von Mises stresses of these ligaments were analyzed.

2.4.4 Model validation

The FE model was validated by comparing the foot contact pressures between FE prediction and in-vivo measurements under three insole conditions during balanced standing. The plantar area was divided into eight parts: the medial heel, lateral heel, medial midfoot, lateral midfoot, first metatarsal, second and third metatarsal, fourth and fifth metatarsals, and hallux. The maximum contact pressure in each region was

extracted for analysis. Correlation analysis and Bland-Altman plots were performed to evaluate the agreement between measurements and predictions using 24 data pairs. The Pearson correlation $|r|$ was categorized as weak, moderate, and strong for $|r| \leqslant 0.35$, $0.36 \leqslant |r| \leqslant 0.67$, and $0.68 \leqslant |r| \leqslant 1.0$, respectively [41].

3 Results

3.1 Validation

The foot pressure distributions of the three insoles obtained by the FE model predictions and in-vivo measurements were compared (Fig. 5). The correlation analysis between the model prediction and in-vivo measurement is shown in Fig. 6(A) and 6(B). The correlation analysis showed that the measurement and prediction were significantly and linearly associated ($r = 0.80$; confidence interval: 95%, 0.59-0.91; $p < 0.001$). The Bland-Altman plot showed a mean offset of 4.2 kPa. The offset was not statistically significant ($p = 0.92$). Additionally, the predicted muscle forces were validated by comparing model-simulated muscle activation with the surface EMG. The validation process is included in Supplementary File 2. Based on the validation results, our model prediction was considered reasonable.

3.2 Navicular height

The navicular heights of the three insole types are shown in Fig.7. The distances increased with the arch support height under the balanced standing (74.2 mm in LA, 76.3 mm in NA, and 77.6 mm in HA), first VGRF peak (78.8 mm in LA, 80.1 mm in NA, and 81.7 mm in HA), and VGRF valley conditions (73.9 mm in LA, 76.1 mm in NA, and 77.9 mm in HA). However, for the second VGRF peak, the distances were

approximately equal for the three insole types.

3.3 Foot contact pressures

The predicted plantar contact pressure distributions for the three insole types are shown in Fig. 8. The pressure distribution patterns were similar under the three insole conditions at the three gait instants. For the forefoot area, the peak pressure value for NA was lower than that for HA and LA during balanced standing. The peak forefoot pressure decreased with an increase in the arch support heights at the first VGRF peak and VGRF valley. The midfoot area's peak foot pressure increased with the arch support height under the balanced standing, first VGRF peak, and VGRF valley conditions. In the hindfoot area, NA and LA exhibited higher peak pressures in balanced standing but lower values at the first VGRF peak when compared to HA. Moreover, the peak hindfoot pressure decreased with an increase in the arch support height. However, at the second VGRF peak, the differences in peak foot pressure among the three insole types were relatively small. Further details are shown in Fig. 9.

3.4 Plantar fascia strain distribution

The plantar fascia strain distribution patterns under the three insole conditions are shown in Fig. 10. The regions tied to the foot bones were excluded from the contour. The remaining part of the fascia was divided equally into three parts. In the hindfoot region, the peak strains for NA and HA were lower than those for LA under the balanced standing, first VGRF peak, and VGRF valley conditions. In the distal region, the NA had lower peak strains than those of LA and HA under the balanced standing, first VGRF peak, and VGRF valley conditions. In the middle region, NA exhibited the

lowest peak strain during balanced standing. The peak strain of the middle region increased at the first VGRF peak but decreased at the VGRF valley with an increase in the arch support heights. For the second VGRF peak, the differences in peak plantar fascia values were relatively small at the three arch support heights. Further details are presented in Fig. 11.

3.5 Major ligaments stresses

The predicted von Mises stresses of the foot ligaments at the three arch heights are compared in Fig. 12. Under the standing condition, most ligament peak stress values were lower in NA, except for those of talonavicular ligaments, when compared to LA and HA. At the first VGRF peak, most ligaments' peak stress values exhibited a decreasing trend with the increase in the arch height support. In the VGRF valley, the peak stress values decreased for the calcaneocuboid, calcaneonavicular, long plantar, and cuboideonavicular ligaments, but decreased for the deltoid and talonavicular ligaments with an increase in the arch support height.

4. Discussion

AAF can cause foot deformity, lower limb pain, and loss of locomotion ability in end-stage patients [42]. Although foot orthosis with arch support has been widely used for flatfoot treatment, an inappropriate foot orthosis design could affect the functional outcomes of orthotic treatment [7]. To investigate the influence of different arch supports, an FE flatfoot model with a 3D plantar fascia was developed, which could demonstrate the internal foot biomechanics during walking. The significance of this study lies in its potential to reveal the loading states of plantar fascia and foot contact

pressure in orthotic treatment, thus assisting foot orthosis design and foot pain relief [17]. This study also detailed the 3D geometry of the plantar fascia contemplating the fascia-bulk soft tissue interaction and considered the muscle force to drive the FE model, which could improve the accuracy of the prediction.

Foot orthosis with arch support has been clinically used to maintain the medial longitudinal arch during weight-bearing conditions [12]. The results of this study indicated that arch support increased the arch height during static condition with an increase in the support height, which is in line with a previous study [21]. As the arch support mainly acted on the navicular (midfoot region), increased support height could induce higher medial midfoot contact pressures during early stance (first VGRF peak) to midstance (VGRF valley). This study further indicated that HA could produce higher peak midfoot pressures under the first VGRF peak and VGRF valley conditions when compared to LA and NA. Excessive medial midfoot pressures originating from HA could cause discomfort under repeated loading, which should be avoided in arch support design [21]. Further, insole materials can affect foot pressure distribution and arch height. Harder insole material can lead to a higher foot arch height and peak foot pressure [21]. Therefore, the interaction of the insole shape and materials should be considered in insole optimization for flatfoot patients.

This study indicated that increased arch support decreased the strain in the proximal region of the plantar fascia during the balanced standing condition. As the progression of flatfoot deformity could increase the plantar fascia strain and may cause plantar fasciitis [43], the reduced plantar fascia strain in the hindfoot area could account

16

for pain relief in proximal regions. However, the middle or distal plantar fascia loading in HA increased when compared to NA during balanced standing, which could also be observed under the first VGRF peak and VGRF loading conditions. The biomechanical changes could be included in flatfoot insole optimization, particularly in patients with pain in various plantar fascia sites. For NA, the customized arch height parameter was determined according to the navicular height. An increased arch support height indicates more forces between the insole and medial midfoot. With the fascia-bulk soft tissue and fascia-bone interactions, the effects of the arch support on the plantar fascia can be divided into two aspects. First, higher arch support could increase the medial longitudinal arch height and reduce the plantar fascia loading. Second, the supporting force induced by the ground or insole interface could load the plantar fascia through the fascia and bulk soft tissue interface, which could not be represented by the simplifications in previous studies [17, 21, 32]. Previous simplified plantar fascia settings could either fail to predict the internal force distribution and explain the plantar aponeurosis twisting [24] or underestimate the plantar fascia loading by 17.7% [26]. The improvement in the model could better represent the external loading on ligamentous structures, thus benefiting the orthotic design in flatfoot.

In addition to the plantar fascia, certain passive structures, such as the short plantar ligament, long plantar ligament, and plantar calcaneonavicular ligament, were also significant in maintaining the static medial longitudinal arch [44]. The results indicated that the maximum stresses of the calcaneonavicular and long plantar ligaments were lower in NA than in LA and HA during the balanced standing condition. However,

during the stance phase, the height of arch support had a relatively small effect on these ligaments. When compared to balanced standing, foot muscles could be more significant in maintaining the dynamic arch [27], which could account for the relatively small differences in ligament loading.

The proposed muscle-driven FE flatfoot model adopted muscle forces to drive the FE models, similar to some studies that focused on barefoot conditions [25, 45]. The predicted muscle forces were validated by comparing model-predicted muscle activation with the corresponding EMG signals adopted in most studies [46, 47]. The predicted peak Achilles tendon (gastrocnemius and soleus) loadings ranged from 3.91 to 3.96 body weight (BW), which were comparable with the validated Achilles tendon loading at a similar walking speed in a previous study [48]. This study adopted a muscle-driven foot model to investigate the effects of foot orthosis on internal foot mechanics during stance, and the dynamic foot biomechanics could be predicted. The predicted peak pressures in the first VGRF peak (0.244 - 0.257 MPa) and the VGRF valley (0.159 - 0.182 MPa) were lower than the measurements reported in a previous study with an integrated musculoskeletal and FE model [45], but overall higher than measurements reported in another study [25]. Previous integrated musculoskeletal and FE models focused on the barefoot condition, which resulted in different results from this study [25, 45]. Other factors, such as plantar fascia setting, materials, and participant variances, could also account for this difference. Nevertheless, the muscle-driven approach was first used in the foot-orthosis model, which could provide more comprehensive dynamic information in orthosis design when compared to previous

foot-orthosis FE models [17, 20, 21].

Several limitations of this study should be noted for the predicted results and further applications. First, the single-subject design for the FE analysis was employed in this study, which could not account for population variances (arch height, BW, foot stiffness, and foot symptoms). However, single-subject models have often been used under a specific set of load situations because the creation of a foot-ankle complex involves highly complex foot structures and loading conditions [49]. Further work should be conducted to consider the patient variances [44]. Second, the material properties of the bony and ligamentous structures in this study were extracted from previous studies [22]. The simplification of the material properties may weaken the individual characteristics. Third, the foot muscles were represented by a one-dimensional string in the foot model, which could not account for muscle-tissue interaction and the change in fiber alignment (or muscle force direction) during a dynamic situation [50]. Fourth, the foot in the musculoskeletal model was modeled as a rigid segment; a more detailed foot model could be used to obtain the internal foot mechanics [51], thus providing more reliable foot muscle forces and internal foot motions for the FE model. Fifth, only static pressures were adopted to validate the FE simulation; dynamic foot-insole pressures or direct internal biomechanics measurements [52] should be considered to improve model prediction accuracy.

5. Conclusion

In this study, the effects of foot orthosis with three arch support heights on internal foot mechanics during the stance phase were investigated by constructing a muscle-

driven FE flatfoot model. The breakthrough of this model was that it enabled a 3D representation of the plantar fascia and its interactions with surrounding osteotendinous structures. The results indicated that plantar fascia stress and strains in the proximal regions could be reduced as the arch support height increased. However, the higher arch support could also increase the medial midfoot contact pressures and the plantar fascia loading in certain regions. The proposed model could contribute to the development of the orthotic design in subject-specific flatfoot deformity interventions, particularly for flatfoot patients with plantar fasciitis.

Ethics statement

The experimental protocol was approved by the Human Subjects Ethics Sub-Committee of the Hong Kong Polytechnic University. The participant was informed of the procedures for data collection and research contents and signed the consent form.

Declaration of competing interest

The authors declare that they have no conflict of interest.

REFERENCES

[1] D.H. Richie, Jr., Biomechanics and clinical analysis of the adult acquired flatfoot, Clin Podiatr Med Surg, 24 (2007) 617-644.

[2] B.J. Munro, J.R. Steele, Foot-care awareness. A survey of persons aged 65 years and older, J Am Podiatr Med Assoc, 88 (1998) 242-248.

[3] S. Pita-Fernandez, C. Gonzalez-Martin, F. Alonso-Tajes, T. Seoane-Pillado, S. Pertega-Diaz, S. Perez-Garcia, R. Seijo-Bestilleiro, V. Balboa-Barreiro, Flat Foot in a Random Population and its Impact on Quality of Life and Functionality, J Clin Diagn Res, 11 (2017) LC22-LC27.

[4] S. Lauterbach, K. Kostev, R. Becker, Characteristics of diabetic patients visiting a podiatry practice in Germany, Journal of wound care, 19 (2010) 140-148.

[5] Y. Kosashvili, T. Fridman, D. Backstein, O. Safir, Y. Bar Ziv, The correlation between pes planus and anterior knee or intermittent low back pain, Foot Ankle Int, 29 (2008) 910-913.

[6] H.A. Banwell, S. Mackintosh, D. Thewlis, Foot orthoses for adults with flexible pes planus: a systematic review, J Foot Ankle Res, 7 (2014) 23.

[7] N. Rasenberg, H. Riel, M.S. Rathleff, S.M.A. Bierma-Zeinstra, M. van Middelkoop, Efficacy of foot orthoses for the treatment of plantar heel pain: a systematic review and meta-analysis, Br J Sports Med, 52 (2018) 1040-1046.

[8] G. Desmyttere, M. Hajizadeh, J. Bleau, M. Begon, Effect of foot orthosis design on lower limb joint kinematics and kinetics during walking in flexible pes planovalgus: A systematic review and meta-analysis, Clin. Biomech., 59 (2018) 117-129.

[9] L.M. Gordillo-Fernández, M. Ortiz-Romero, J. Valero-Salas, J.L. Salcini-Macías, S. Benhamu-Benhamu, R. García-de-la-Peña, J.A. Cervera-Marin, Effect by custom-made foot orthoses with added support under the first metatarso-phalangeal joint in hallux limitus patients: Improving on first metatarso-phalangeal joint extension, Prosthet Orthot Int, 40 (2016) 668-674.

[10] R. Xu, Z. Wang, Z. Ren, T. Ma, Z. Jia, S. Fang, H. Jin, Comparative Study of the Effects of Customized 3D printed insole and Prefabricated Insole on Plantar Pressure and Comfort in Patients with Symptomatic Flatfoot, Med Sci Monit, 25 (2019) 3510-3519.

[11] A. Hirschmüller, H. Baur, S. Müller, P. Helwig, H.H. Dickhuth, F. Mayer, Clinical effectiveness of customised sport shoe orthoses for overuse injuries in runners: a randomised controlled study, Br J Sports Med, 45 (2011) 959-965.

[12] G. Wahmkow, M. Cassel, F. Mayer, H. Baur, Effects of different medial arch support heights on rearfoot kinematics, PLOS ONE, 12 (2017) e0172334.

[13] Y. Peng, D.W. Wong, Y. Wang, T.L. Chen, Q. Tan, Z. Chen, Z. Jin, M. Zhang, Immediate Effects of Medially Posted Insoles on Lower Limb Joint Contact Forces in Adult Acquired Flatfoot: A Pilot Study, Int J Environ Res Public Health, 17 (2020).

[14] A. Erdemir, A.J. Hamel, A.R. Fauth, S.J. Piazza, N.A. Sharkey, Dynamic loading of the plantar aponeurosis in walking, J Bone Joint Surg Am, 86 (2004) 546-552.

[15] G.F. Kogler, S.E. Solomonidis, J.P. Paul, In vitro method for quantifying the effectiveness of the longitudinal arch support mechanism of a foot orthosis, Clin Biomech (Bristol, Avon), 10 (1995) 245-252.

[16] Y. Wang, D.W.-C. Wong, M. Zhang, Computational Models of the Foot and Ankle for Pathomechanics and Clinical Applications: A Review, Ann. Biomed. Eng., 44 (2016) 213-221.

[17] Y.C. Hsu, Y.W. Gung, S.L. Shih, C.K. Feng, S.H. Wei, C.H. Yu, C.S. Chen, Using an optimization

approach to design an insole for lowering plantar fascia stress--a finite element study, Ann Biomed Eng, 36 (2008) 1345-1352.

[18] W.-M. Chen, S.-J. Lee, P.V.S. Lee, Plantar pressure relief under the metatarsal heads – Therapeutic insole design using three-dimensional finite element model of the foot, J. Biomech., 48 (2015) 659-665.

[19] J.T.-M. Cheung, M. Zhang, Parametric design of pressure-relieving foot orthosis using statistics-based finite element method, Med Eng Phys, 30 (2008) 269-277.

[20] H. Zhang, M.L. Lv, J. Yang, W. Niu, J. Chung-Wai, Computational Modelling of Foot Orthosis for Midfoot Arthritis: A Taguchi Approach for Design Optimization,2020. Acta Bioeng Biomech.

[21] S. Su, Z. Mo, J. Guo, Y. Fan, The Effect of Arch Height and Material Hardness of Personalized Insole on Correction and Tissues of Flatfoot, J. Healthc. Eng., 2017 (2017) 8614341.

[22] H.Y. Cheng, C.L. Lin, H.W. Wang, S.W. Chou, Finite element analysis of plantar fascia under stretch-the relative contribution of windlass mechanism and Achilles tendon force, J Biomech, 41 (2008) 1937-1944.

[23] J. Yu, D.W.-C. Wong, H. Zhang, Z.-P. Luo, M. Zhang, The influence of high-heeled shoes on strain and tension force of the anterior talofibular ligament and plantar fascia during balanced standing and walking, Med Eng Phys, 38 (2016) 1152-1156.

[24] Y.-N. Chen, C.W. Chang, C.T. Li, C.H. Chang, C.F. Lin, Finite element analysis of plantar fascia during walking: a quasi-static simulation, Foot Ankle Int, 36 (2015) 90-97.

[25] M. Akrami, Z. Qian, Z. Zou, D. Howard, C.J. Nester, L. Ren, Subject-specific finite element modelling of the human foot complex during walking: sensitivity analysis of material properties, boundary and loading conditions, Biomech Model Mechan, 17 (2018) 559-576.

[26] Y. Peng, D. Wai-Chi Wong, Y. Wang, T. Lin-Wei Chen, G. Zhang, F. Yan, M. Zhang, Computational Models of Flatfoot with Three-dimensional Fascia and Bulk Soft Tissue Interaction for Orthosis Design, Medicine in Novel Technology and Devices, (2020) 100050.

[27] T.L. Chen, D.W. Wong, Y. Wang, J. Lin, M. Zhang, Foot arch deformation and plantar fascia loading during running with rearfoot strike and forefoot strike: A dynamic finite element analysis, J Biomech, 83 (2019) 260-272.

[28] M. Mueller, J. Host, B. Norton, Navicular drop as a composite measure of excessive pronation, Journal of the American Podiatric Medical Association, 83 (1993) 198-202.

[29] H. Roy, K. Bhattacharya, S. Deb, K. Ray, Arch index: an easier approach for arch height (a regression analysis), Al Ameen J Med Sci, 5 (2012) 137-146.

[30] M. Damsgaard, J. Rasmussen, S.T. Christensen, E. Surma, M. De Zee, Analysis of musculoskeletal systems in the AnyBody Modeling System, Simulation Modelling Practice and Theory, 14 (2006) 1100-1111.

[31] M.K. Horsman, H.F. Koopman, F.C. van der Helm, L.P. Prosé, H. Veeger, Morphological muscle and joint parameters for musculoskeletal modelling of the lower extremity, Clin. Biomech., 22 (2007) 239-247.

[32] D.W.-C. Wong, Y. Wang, A.K.-L. Leung, M. Yang, M. Zhang, Finite element simulation on posterior tibial tendinopathy: Load transfer alteration and implications to the onset of pes planus, Clin. Biomech., 51 (2018) 10-16.

[33] D.G. Wright, D.C. Rennels, A Study of the Elastic Properties of Plantar Fascia, JBJS, 46 (1964),482-492.

[34] S. Siegler, J. Block, C.D. Schneck, The Mechanical Characteristics of the Collateral Ligaments of the Human Ankle Joint, Foot & ankle, 8 (1988) 234-242.

[35] D. Lemmon, T.Y. Shiang, A. Hashmi, J.S. Ulbrecht, P.R. Cavanagh, The effect of insoles in therapeutic footwear—A finite element approach, J. Biomech., 30 (1997) 615-620.

[36] W.-P. Chen, C.-W. Ju, F.-T. Tang, Effects of total contact insoles on the plantar stress redistribution: a finite element analysis, Clin. Biomech., 18 (2003) S17-S24.

[37] C. Pailler-Mattei, S. Bec, H. Zahouani, In vivo measurements of the elastic mechanical properties of human skin by indentation tests, Med Eng Phys, 30 (2008) 599-606.

[38] W.-M. Chen, T. Lee, P.V.-S. Lee, J.W. Lee, S.-J. Lee, Effects of internal stress concentrations in plantar soft-tissue—A preliminary three-dimensional finite element analysis, Med Eng Phys, 32 (2010) 324-331.

[39] G. Lewis, Finite element analysis of a model of a therapeutic shoe: effect of material selection for the outsole, Biomed Mater Eng, 13 (2003) 75-81.

[40] H.B. Henninger, S.P. Reese, A.E. Anderson, J.A. Weiss, Validation of computational models in biomechanics, Proc Inst Mech Eng H, 224 (2010) 801-812.

[41] R. Taylor, Interpretation of the correlation coefficient: a basic review, J Diagn Med Sonogr, 6 (1990) 35-39.

[42] S.-Y. Park, H.-S. Bang, D.-J. Park, Potential for foot dysfunction and plantar fasciitis according to the shape of the foot arch in young adults, J Exerc Rehabil, 14 (2018) 497-502.

[43] D.B. Irving, J.L. Cook, H.B. Menz, Factors associated with chronic plantar heel pain: a systematic review, J Sci Med Sport, 9 (2006) 11-22.

[44] D. Richie, Biomechanics and Orthotic Treatment of the Adult Acquired Flatfoot, Clin Podiatr Med Sur, 37 (2020) 71-89.

[45] A. Scarton, A. Guiotto, T. Malaquias, F. Spolaor, G. Sinigaglia, C. Cobelli, I. Jonkers, Z. Sawacha, A methodological framework for detecting ulcers' risk in diabetic foot subjects by combining gait analysis, a new musculoskeletal foot model and a foot finite element model, Gait Posture, 60 (2018) 279-285.

[46] J.L. Hicks, T.K. Uchida, A. Seth, A. Rajagopal, S.L. Delp, Is My Model Good Enough? Best Practices for Verification and Validation of Musculoskeletal Models and Simulations of Movement, J Biomech Eng, 137 (2015) 020905.

[47] T.L.-W. Chen, D.W.-C. Wong, Z. Xu, Q. Tan, Y. Wang, A. Luximon, M. Zhang, Lower limb muscle co-contraction and joint loading of flip-flops walking in male wearers, PLOS ONE, 13 (2018) e0193653.

[48] E.M. Keuler, I.F. Loegering, J.A. Martin, J.D. Roth, D.G. Thelen, Shear Wave Predictions of Achilles Tendon Loading during Human Walking, Sci Rep, 9 (2019) 1-9.

[49] T.L.-W. Chen, D.W.-C. Wong, Y. Peng, M. Zhang, Prediction on the plantar fascia strain offload upon Fascia taping and Low-Dye taping during running, J Orthop Transla, 20 (2020) 113-121.

[50] J. Li, Y. Lu, S.C. Miller, Z. Jin, X. Hua, Development of a finite element musculoskeletal model with the ability to predict contractions of three-dimensional muscles, J. Biomech., 94 (2019) 230-234.

[51] M. Oosterwaal, S. Telfer, S. Tørholm, S. Carbes, L.W. van Rhijn, R. Macduff, K. Meijer, J. Woodburn, Generation of subject-specific, dynamic, multisegment ankle and foot models to improve orthotic design: a feasibility study, BMC Musculoskelet Disord, 12 (2011) 1-10.

[52] B. H., N. T., V.D. C., C. W., D. G., J. I., V.S. J., Combination of 4D CT scanning and a foot manipulator device to measure individual foot kinematics during simulated gait, Orthopaedic Proceedings, 99-B (2017) 9-9.

.
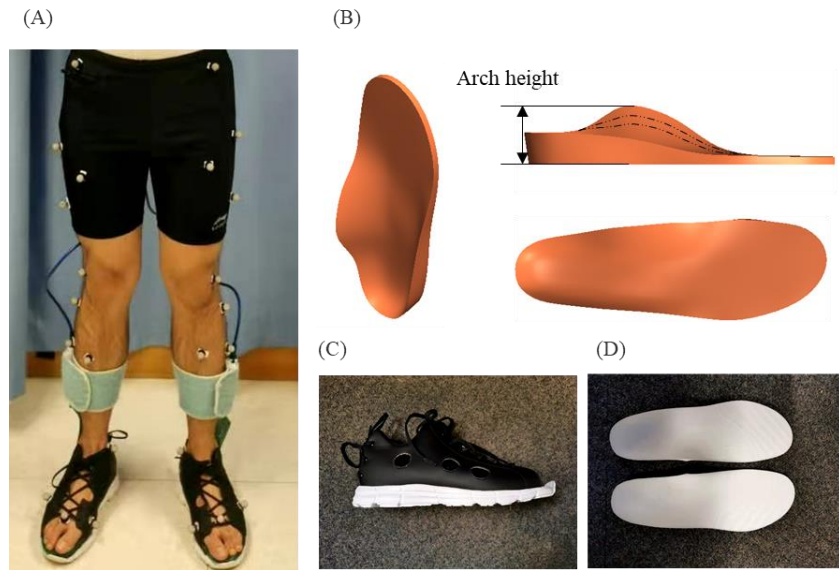
Fig. 1. Experimental setup for the data collection, including (A) markers and foot pressure sensors configuration, (B) foot orthosis with different arch support heights, (C) lateral view of the shoe, (D) 3D printing insoles.
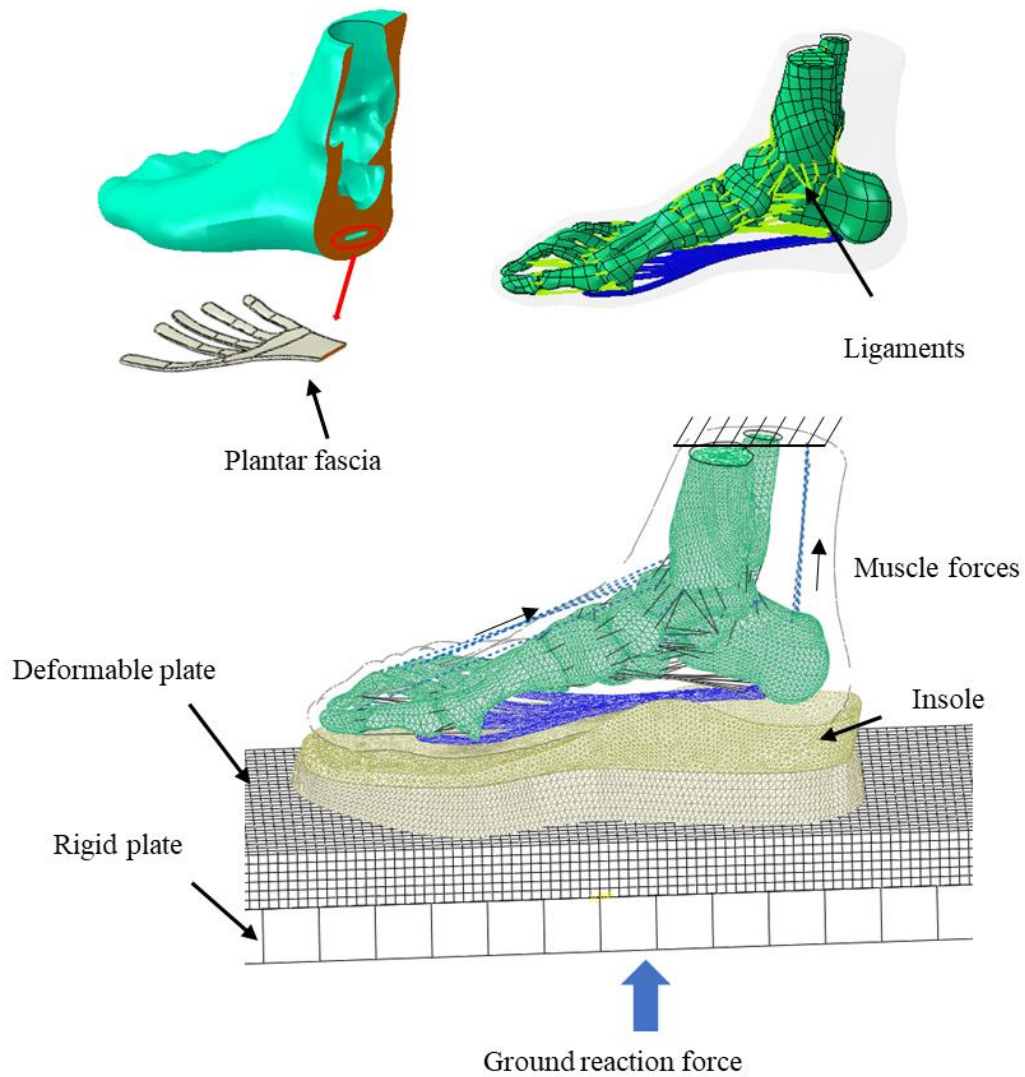
Fig. 2. Overview of the foot-ankle complex and insole finite element model. The bulk soft tissue (transparent) was constructed by subtracting plantar fascia and bony structures' geometry. The interior surface of the encapsulated soft tissue was tied to the bony structures. The skin layer was defined as a 2-mm thick membrane encapsulated the bulk soft tissue. And the three-dimension plantar fascia were tied to the calcaneal tubercle, the proximal phalanges, and the surrounding soft tissues. The proximal cross-section surface of the tibia, fibula, and skin was fixed. One rigid plate was tied to the deformable plate, and the motion and force were applied on the rigid plate. The foot muscle, including tibialis anterior, tibialis posterior, peroneus brevis, peroneus longus, Achilles tendon (gastrocnemius and soleus), flexor hallucis longus, and flexor digitorum longus, were modelled as connectors. These muscle forces were applied to foot FE model through the connectors.
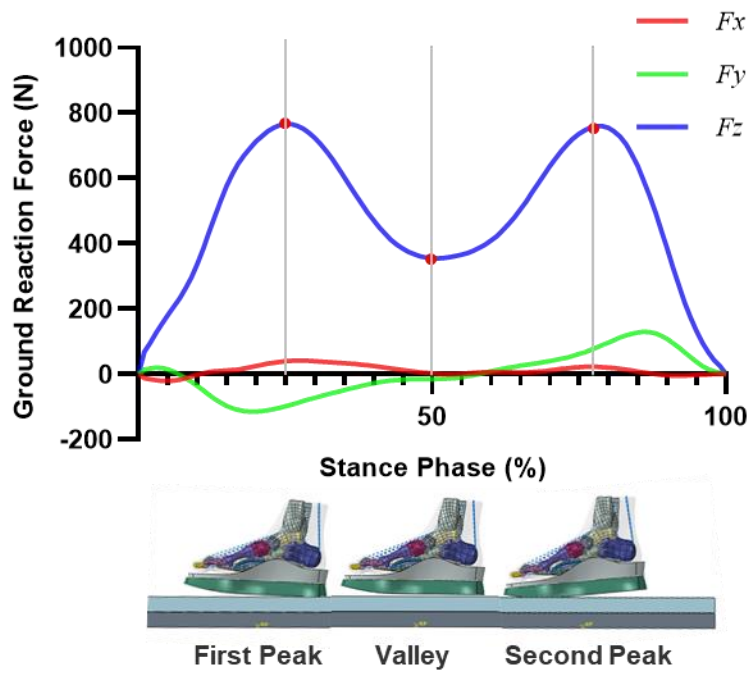
Fig. 3. An illustration of the three gait instants from the vertical ground reaction forces during the stance phase.
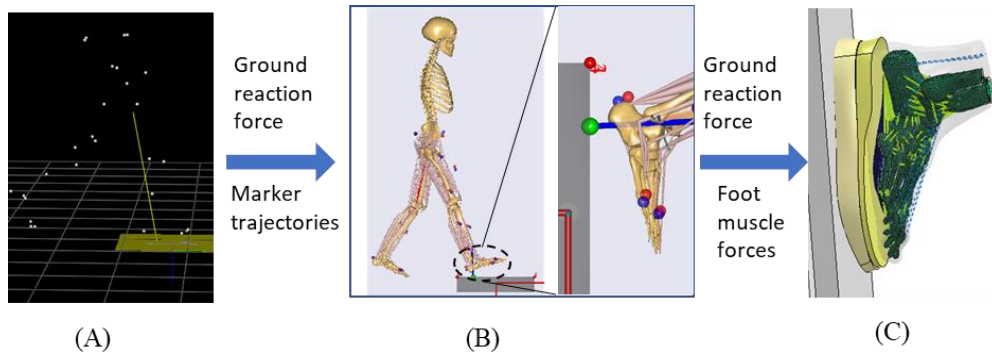
Fig. 4. The workflow of the muscle-driven finite element model, including (A) gait data collection, (B) musculoskeletal multibody model, (C) finite element foot model
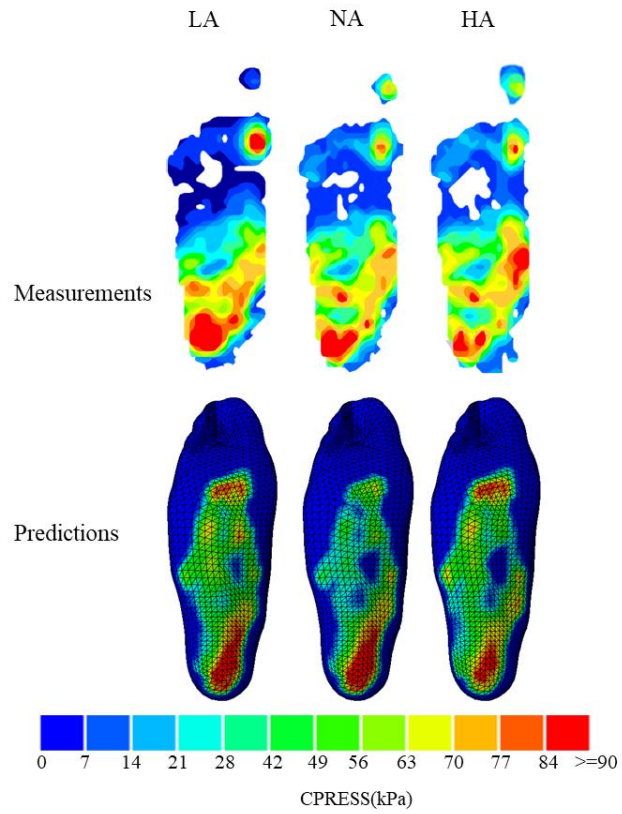
Fig. 5. Comparison of foot pressure distribution between model predictions and measurements of three arch support heights in balanced standing. LA, NA and HA represent foot orthosis with three arch support heights (low, neutral and high).
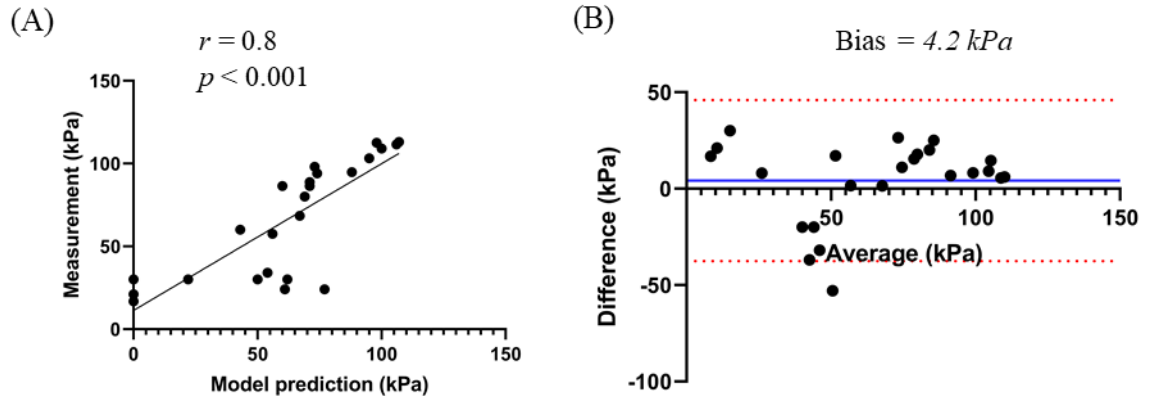
Fig. 6. Validation of finite element model with experimental measurement using (A) correlation analysis; and (B) the Bland-Altman plot. Blue line represents the mean difference. And red lines are the 95% confidence interval.
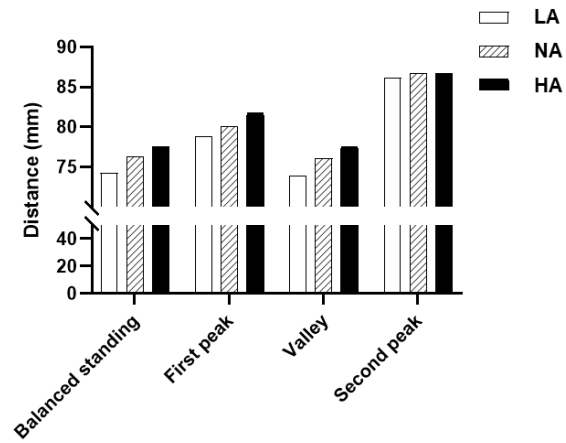
Fig. 7. Distance between navicular and ground in foot orthosis with three arch support heights in balanced standing and three gait instants. LA, NA and HA represent foot orthosis with three arch support heights (low, neutral and high).
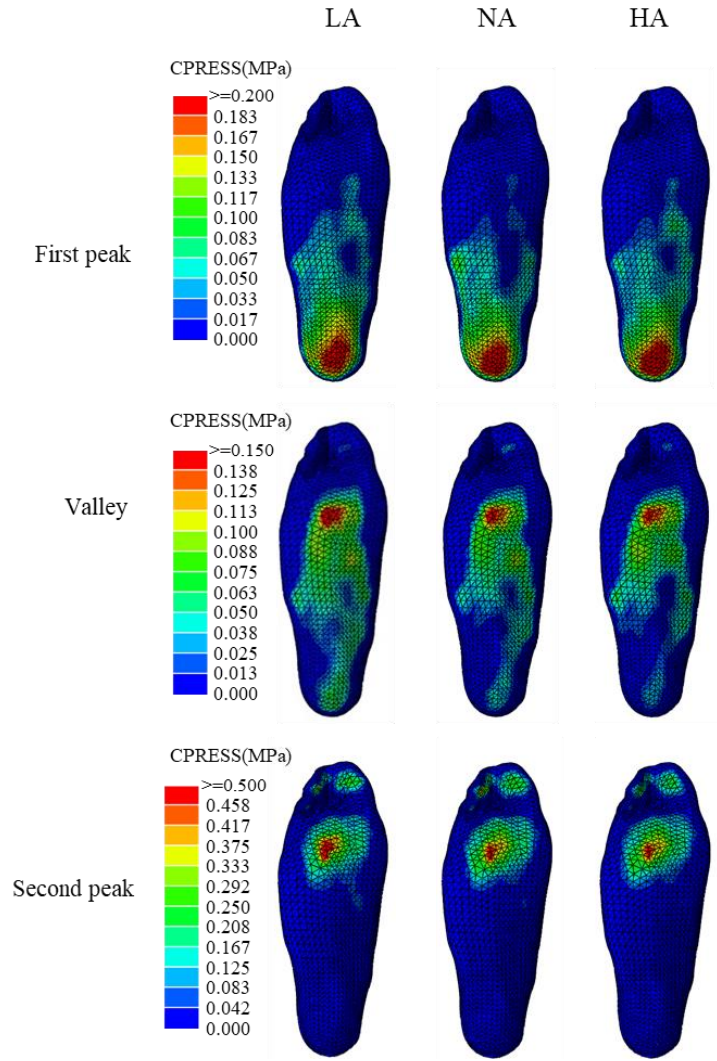
Fig. 8. Comparison of the foot pressure distributions among three insole conditions in three gait instants, including first peak VGRF, VGRF valley, and second peak VGRF. LA, NA and HA represent foot orthosis with three arch support heights (low, neutral and high).
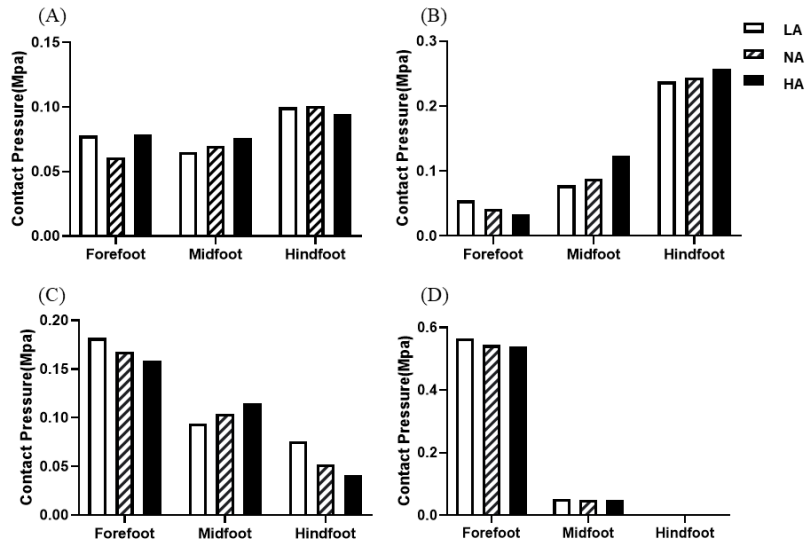
Fig. 9. Comparison of peak foot plantar pressure of forefoot, midfoot and hindfoot of three insole conditions in balanced standing and three gait events, (A) balanced standing, (B) first peak VGRF, (C) VGRF valley, and (D) second peak VGRF. LA, NA and HA represent foot orthosis with three arch support heights (low, neutral and high).
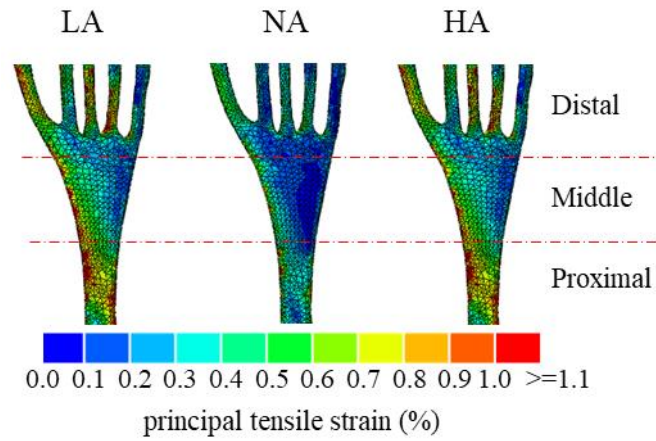
Fig. 10. Strain contour of the plantar fascia in foot orthosis with three arch support heights. The region that was close to the foot bone was excluded from the contour. The fascia's remaining part is divided equally into three parts: proximal, middle, and distal parts. LA, NA and HA represent foot orthosis with three arch support heights (low, neutral and high).
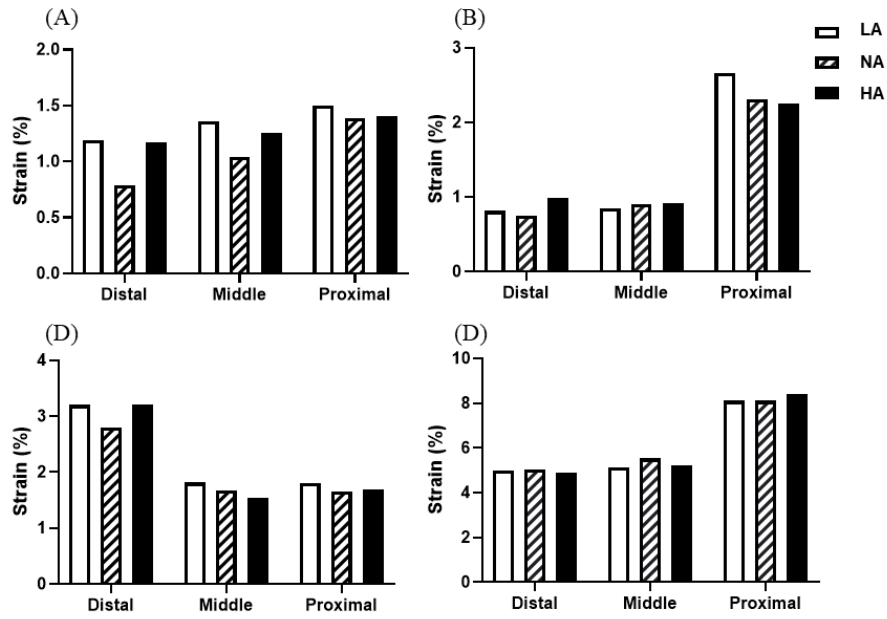
Fig. 11. Comparison of peak plantar fascia for three insole conditions in balanced standing and three gait events, (A) balanced standing, (B) first peak GRF, (C) GRF valley, and (D) second peak GRF. LA, NA and HA represent foot orthosis with three arch support heights (low, neutral and high).
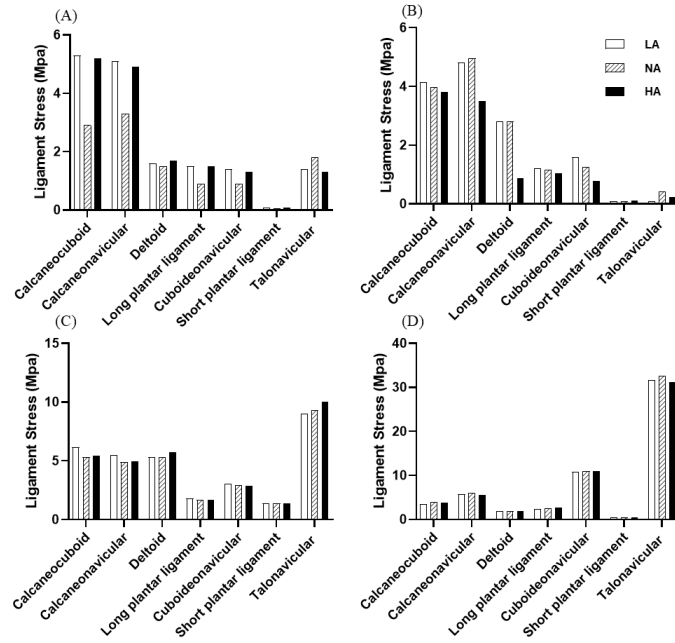
Fig. 12. Comparison of peak ligaments Von stress for three insole conditions in balanced standing and three gait events, (A) balanced standing, (B) first peak GRF, (C) GRF valley, and (D) second peak GRF.

Table 1. Material properties of the components in the finite element model

	Elastic modulus (MPa)	Poisson ratio	Cross-section (mm^2)	References
Skin	1st-order Ogden hyperelastic model (μ= 0.122 MPa, α=18, Thickness: 2.0 mm)		-	[37]
Bulk soft tissue	second-order polynomial strain hyperelastic model (C_{10}=0.8556, C_{01}=-0.05841, C_{20}=0.03900, C_{11}=-0.02319, C_{02}=0.00851, D_1=3.65273)		-	[35]
Bone	10000	0.34	-	[36]
Ligaments	260	0.4	18.4	[34]
Three-dimensional Plantar fascia	350	0.45	-	[33]
Insole	7.8	0.35	-	-
Midsole	5	0.4	-	[39]